*Inorg. Chem.* **2005**, *44*, 1367−1380


# Fe–N–O Structure and Bonding in Six-Coordinate {FeNO}$^6$ Porphyrinates Containing Imidazole: Implications for Reactivity of Coordinated NO

**Douglas P. Linder and Kenton R. Rodgers***

*Department of Chemistry, Biochemistry, and Molecular Biology, North Dakota State University, Fargo, North Dakota 58105-5516*

Received July 19, 2004

We report density functional theory calculations on six-coordinate ferric-NO ({FeNO}$^6$) porphyrinates that contain either imidazole or imidazolate as the trans axial ligand. Our results show that the sensitivities of the Fe–NO and N–O stretching frequencies to cis and trans influences are *directly* correlated. In other words, as one decreases so does the other for both the imidazole and the imidazolate complexes. This correlation is opposite that of the isoelectronic ferrous-CO systems, whose Fe–CO and C–O frequencies are well-known to be *inversely* correlated. Based on the results of our calculations, the molecular origin of the *direct* correlation in {FeNO}$^6$ porphyrinates can be explained by trends in the electron density distributions within the HOMO or HOMO–1, which exhibits Fe–NO and N–O $\pi$-antibonding character. Variability in the Fe–N–O $\pi$-antibonding character of the HOMO or the HOMO–1 modulates the ∠FeNO as well as the Fe–NO and N–O bond strengths in concert. Orbital interactions in the six-coordinate Fe$^{III}$NO porphyrin complexes are compared and contrasted with those of the isoelectronic Fe$^{II}$CO analogues, and an overall view of {FeNO}$^6$ bonding in these complexes is set forth.

## Introduction

Nitric oxide (NO) is involved in a number of important biological functions in higher organisms, including neurotransmission, vasodilation, and blood clotting.[1−4] Additionally, NO complexes of heme iron and copper are crucial to bacterial and fungal denitrification reactions wherein NO is reduced to $N_2O$.[5] An interesting feature of NO, which distinguishes it from CO and $O_2$, is its affinity for heme proteins in both their ferrous and ferric oxidation states to yield the ferrous and ferric NO adducts, {FeNO}$^7$ and {FeNO}$^6$, respectively.[6−8]

In a previous study on five-coordinate {FeNO}$^6$ porphyrin complexes, we observed a *direct* correlation between the $\nu_{Fe-NO}$ and $\nu_{N-O}$ frequencies, as determined by resonance Raman scattering and IR absorbance methods.[9] That is, factors that affect the FeNO triatomic unit either increase or decrease the strengths of both the Fe−NO and N−O bonds. This correlation is opposite that observed for the isoelectronic [Fe$^{II}$CO] complexes, as well as the {FeNO}$^7$ and [Fe$^{II}$O$_2$] systems.[10,11] For the five-coordinate {FeNO}$^6$ porphyrinates, the sensitivity of the FeNO bonding was analyzed using density functional theory (DFT) calculations on a series of complexes whose electronic properties were modulated by modification of the porphyrin periphery.[9] Those calculations

* To whom correspondence should be addressed. E-mail: Kent.Rodgers@ndsu.nodak.edu.

(1) Culotta, E.; Koshland, D. E., Jr. *Science* **1992**, *258*, 1862−1865.
(2) Cooper, C. E. *Biochim. Biophys. Acta* **1999**, *1411*, 290−309.
(3) *Methods in Nitric Oxide Research*; Feelisch, M., Stamler, J. S., Eds.; Wiley: Chichester, 1996.
(4) McCleverty, J. A. *Chem. Rev.* **2004**, *104*, 403−418.
(5) Wasser, I. M.; de Vries, S.; Moenne-Loccoz, P.; Schroder, I.; Karlin, K. D. *Chem. Rev.* **2002**, *102*, 1201−1234.
(6) The {FeNO}$^n$ nomenclature of Enemark and Feltham is used here since the assignment of oxidation states for NO-coordinated complexes is not unambiguous. In {FeNO}$^n$ the *n* represents the number of iron atom d-electrons plus the lone $\pi$* electron from the nitrosyl ligand. Using this nomenclature the "ferric" or Fe(III) nitrosyl systems are classified as {FeNO}$^6$, whereas the "ferrous" or Fe(II) nitrosyls are classified as {FeNO}$^7$ systems. Enemark, J. H.; Feltham, R. D. *Coord. Chem. Rev.* **1974**, *13*, 339−406.
(7) Wyllie, G. R. A.; Scheidt, W. R. *Chem. Rev.* **2002**, *102*, 1067−1089.
(8) Jain, R.; Chan, M. K. *J. Biol. Inorg. Chem.* **2003**, *8*, 1−11.
(9) Linder, D. P.; Rodgers, K. R.; Banister, J.; Wyllie, G. R. A.; Ellison, M. K.; Scheidt, W. R. *J. Am. Chem. Soc.* **2004**, *126*, 14136−14148.
(10) (a) Spiro, T. G.; Zgierski, M. Z.; Kozlowski, P. W. *Coord. Chem. Rev.* **2001**, *219−221*, 923−936. (b) Coyle, C. M.; Vogel, K. M.; Rush, T. S., III; Kozlowski, P. M.; Williams, R.; Spiro, T. G.; Dou, Y.; Ikeda-Saito, M.; Olson, J. S.; Zgierski, M. Z. *Biochemistry* **2003**, *42*, 4896−4903.
(11) (a) Vogel, K. M.; Kozlowski, P. M.; Zgierski, M. Z.; Spiro, T. G. *J. Am. Chem. Soc.* **1999**, *121*, 9915−9921. (b) Vogel, K. M.; Kozlowski, P. M.; Zgierski, M. Z.; Spiro, T. G. *Inorg. Chim. Acta* **2000**, *297*, 11−17.

10.1021/ic049045h CCC: $30.25 
Published on Web 01/29/2005

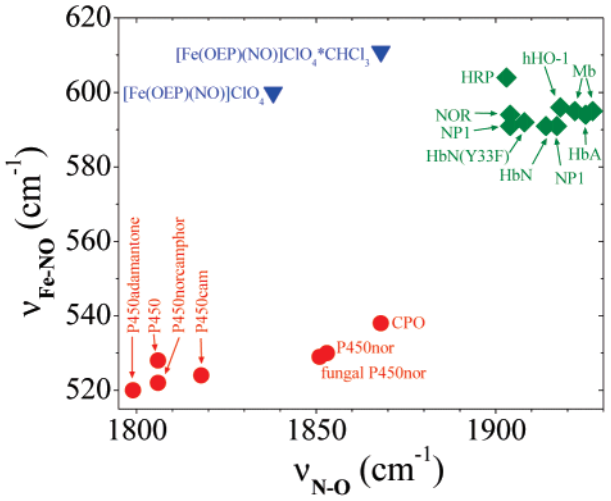


**Figure 1.** Experimental correlations between $\nu_{Fe-NO}$ and $\nu_{N-O}$ frequencies for {FeNO}$^6$ systems constructed from published data. Circles (●), six-coordinate hemes in enzymes having proximal Cys-based thiolate ligands; triangles (▼), five-coordinate complexes; diamonds (◆), six-coordinate hemes in proteins having proximal His-based ImH or Im$^-$ ligands. P450,[12a] CPO,[12] NOR,[20] fungal P450nor,[13] Mb,[14,16,17] HRP,[14,16] NP1,[21] hHO-1,[19] HbA,[14,15] HbN,[18] [Fe(OEP)(NO)]ClO$_4$.[9]

revealed an elegant relationship between the sensitivities of the Fe−NO and N−O bond strengths that clarifies the correlations between $\nu_{Fe-NO}$ and $\nu_{N-O}$ in those five-coordinate complexes. The electronic basis for this behavior is centered around a high-energy molecular orbital which is $\sigma$-antibonding throughout the Fe−N−O triatomic unit. A direct relationship between the experimental Fe−NO and N−O frequencies has also been reported for six-coordinate thiolate-ligated {FeNO}$^6$ hemes.[12a] Hence, the *direct* relationship between the sensitivities of Fe−NO and N−O bond strengths to changes in structure and environment of the complexes is emerging as a general characteristic of {FeNO}$^6$ porphyrin systems.

Figure 1 shows plots of $\nu_{Fe-NO}$ versus $\nu_{N-O}$ correlations for five- and six-coordinate {FeNO}$^6$ porphyrinates constructed using published experimental frequencies. Even from this limited data set, it is evident that a direct correlation exists for both the five-coordinate systems and the six-coordinate enzymes containing a proximal thiolate ligand trans to NO. Although the plots in Figure 1 do not address whether a correlation exists in six-coordinate {FeNO}$^6$ systems that contain an axial (proximal) imidazole ligand, there are indications that the FeNO bond strength sensitivities in these systems are distinct from their $FeO_2$, {FeNO}$^7$, and isoelectronic Fe$^{II}$CO counterparts. For example, in wild-type Mb$^{III}$NO a single $\nu_{N-O}$ band is observed at 1927 cm$^{-1}$. When the distal histidine (H64) is replaced by leucine, this band shifts down in frequency to 1904 cm$^{-1}$.[17] This is counter to the $\nu_{C-O}$ and $\nu_{N-O}$ shifts in the CO and NO complexes of ferrous Mb(H64L), which are observed at over 20 cm$^{-1}$ *higher* in frequency.[22] In the current model for the relationship between Fe−XO and X−O sensitivities in the CO, NO, and $O_2$ adducts of ferrous Mb, H64 exists as the $N_\epsilon$H tautomer, which results in a positive polar ($\delta^+$) or H-bond donor interaction between H64 and the XO ligands.[17,22] It has been suggested that the frequency lowering of $\nu_{N-O}$ in Mb(H64L)$^{III}$NO is due to H64 tautomerization to yield deprotonated $N_\epsilon$, resulting in a negative polar interaction ($\delta^-$) with NO.[17] The premise for this model is that the pattern of Fe−NO and N−O bond sensitivities to environmental changes is the same in the ferrous and ferric systems. However, given that other {FeNO}$^6$ systems exhibit a *direct* correlation in the $\nu_{Fe-NO}$ and $\nu_{N-O}$ frequencies, the presumption of an indirect correlation analogous to that seen in the Fe$^{II}$XO adducts warrants re-evaluation.

Although NO binds to the ferrous state with much greater affinity than the ferric state, {FeNO}$^6$ complexes of heme proteins have significant biological importance. For example, the vasodilating effect of NO in mammals is exploited by the blood-sucking insect *Rhodnius prolixus* which delivers NO to the tissues of its victim as a means of maintaining blood flow to the site of its bite. Delivery of NO is accomplished by the NO adduct of a group of ferric, not ferrous, heme proteins called nitrophorins (NPs), which are contained in the insect's saliva.[21,23,24] The nitrophorins are six-coordinate ferric heme proteins which contain a proximal histidine ligand trans to NO. Other histidine-ligated {FeNO}$^6$ heme proteins that have been characterized include myoglobin (Mb),[11,16,17,25,26] hemoglobin (Hb),[14,15] horseradish peroxidase (HRP),[14,16,27] mammalian heme oxygenase (hHO) isoforms 1[19] and 2,[28] nitric oxide reductase (NOR),[5,20] FixL,[29] and leghemoglobin.[30] While structural and electronic proper-

(12) (a) Obayashi, E.; Tsukamato, K.; Adachi, S.; Takahashi, S.; Nomura, M.; Iizuka, T.; Shoun, H.; Shiro, Y. *J. Am. Chem. Soc.* **1997**, *119*, 7807−7816. (b) Hu, S.; Kincaid, J. R. *J. Biol. Chem.* **1993**, *268*, 6189−6193.
(13) Shimizu, H.; Obayashi, E.; Gomi, Y.; Arakawa, H.; Park, S.-Y.; Nakamura, H.; Adachi, S.-I.; Shoun, H.; Shiro, Y. *J. Biol. Chem.* **2000**, *275*, 4816−4826.
(14) Benko, B.; Yu, N. T. *Proc. Natl. Acad. Sci. U.S.A.* **1983**, *80*, 7042−7046.
(15) Wang, Y.; Averill, B. A. *J. Am. Chem. Soc.* **1996**, *118*, 3972−3973.
(16) Tomita, T.; Haruta, N.; Aki, M.; Kitagawa, T.; Ikeda-Saito, M. *J. Am. Chem. Soc.* **2001**, *123*, 2666−2667.
(17) Miller, L. M.; Pedraza, A. J.; Chance, M. R. *Biochemistry* **1997**, *36*, 12199−12207.
(18) Mukai, M.; Ouellet, Y.; Ouellet, H.; Guertin, M.; Yeh, S.-R. *Biochemistry* **2004**, *43*, 2764−2770.
(19) Wang, J.; Lu, S.; Moenne-Loccoz, P.; Ortiz de Montellano, P. R. *J. Biol. Chem.* **2003**, *278*, 2341−2347.
(20) Pinakoulaki, E.; Gemeinhardt, S.; Saraste, M.; Varotsis, C. *J. Biol. Chem.* **2002**, *277*, 23407−23413.
(21) (a) Ding, X. D.; Weichsel, A.; Anderson, J. F.; Shokhireva, T. Kh.; Balfour, C.; Pierik, A. J.; Averill, B. A.; Montfort, W. R.; Walker, F. A. *J. Am. Chem. Soc.* **1999**, *121*, 128−138. (b) Maes, E. M.; Walker, F. A.; Monfort, W. R.; Czernuszewicz, R. S. *J. Am. Chem. Soc.* **2001**, *123*, 11664−11672.
(22) (a) Phillips, G. N.; Teodoro, M. L.; Li, T.; Smith, B.; Olson, J. S. *J. Phys. Chem. B* **1999**, *103*, 8817−8829. (b) Springer, B. A.; Sligar, S. G.; Olson, J. S.; Phillips, G. N. *Chem. Rev.* **1994**, *94*, 699−714.
(23) Ribeiro, J. M. C.; Hazzard, J. M. H.; Nussenzveig, R. H.; Champagne, D. E.; Walker, F. A. *Science* **1993**, *260*, 539−541.
(24) Roberts, S. A.; Weichsel, A.; Qiu, Y.; Shelnutt, J. A.; Walker, F. A.; Montfort, W. R. *Biochemistry* **2001**, *40*, 11327−11337.
(25) Rich, A. M.; Armstrong, R. S.; Ellis, P. J.; Lay, P. A. *J. Am. Chem. Soc.* **1998**, *120*, 10827−10836.
(26) Moeller, J. K. S.; Skibsted, L. *Chem. Rev.* **2002**, *102*, 1167−1178.
(27) Sono, M.; Roach, M. P.; Coulter, E. D.; Dawson, J. H. *Chem. Rev.* **1996**, *96*, 2841−2888.
(28) Ishikawa, K.; Takeuchi, N.; Takahashi, S.; Mansfield Matera, K.; Sato, M.; Shibahara, S.; Rousseau, D. L.; Ikeda-Saito, M.; Yoshida, T. *J. Biol. Chem.* **1995**, *270*, 6345−6350.
(29) Rodgers, K. R.; Lukat-Rodgers, G. S.; Tang, L. *J. Biol. Inorg. Chem.* **2000**, *5*, 642−654.

ties of {FeNO}$^7$ heme proteins and model complexes have been extensively studied, the {FeNO}$^6$ analogues have received less attention, due perhaps in part to their greater reactivity. The {FeNO}$^6$ porphyrinates are susceptible in varying degrees to reductive nitrosylation, wherein a nucleophile, such as hydroxide ion, is nitrosated by the {FeNO}$^6$ complex with concomitant formation of an Fe(II) center.[7] In the presence of excess NO, the Fe(II) is trapped by formation of the exceedingly stable {FeNO}$^7$ complex.

Our previous study clearly showed that, in addition to the direct relationship between the relative susceptibilities of the Fe−NO and N−O bond strengths to peripheral and distal effects, their *absolute* sensitivities to these effects are substantially larger than those of their [Fe$^{II}$CO] and {FeNO}$^7$ counterparts. In other words, FeNO bonding in the {FeNO}$^6$ porphyrinates appears to be sufficiently sensitive to structural and environmental factors that the *reactivity* of bound NO can be modulated. Thus, in addition to ferric hemes having lower affinity for NO, as in the aforementioned example of the nitrophorins, this malleability of {FeNO}$^6$ reactivity is also tied to variable electrophilicity of the bound NO nitrogen atom. The reactivity of bound NO toward nucleophiles such as hydroxide, leading to reductive nitrosylation (NO oxidation), and hydride, leading to NO reduction, is thereby regulated. Given that these reactions of coordinated NO proceed through six-coordinate {FeNO}$^6$ heme centers, we have undertaken the present study with the aim of clarifying the role of proximal heme ligation by imidazole (ImH) and imidazolate (Im$^-$) in the modulation of FeNO bonding and reactivity.

This report describes the structural and electronic effects, as determined using computational methods based on density functional theory, of systematically varying *meso* and $\beta$-pyrrole substituents of six-coordinate {FeNO}$^6$ porphyrinates containing either ImH or Im$^-$ ligands trans to NO (Figure 2). The {FeNO}$^6$−ImH and {FeNO}$^6$−Im$^-$ models represent the extremes of proximal charge that the protein environment can impose on proximal His ligands, that is, no H-bonding and strong H-bond donation by the bound His. The DFT results indeed show a *direct* correlation between the Fe−NO and N−O bond strengths for both the ImH and Im$^-$ systems, further suggesting the *direct* correlation is an innate property of the {FeNO}$^6$ porphyrinates. Furthermore, the Kohn−Sham molecular orbitals reveal the origin of the *direct* correlation. For both the ImH and Im$^-$ systems, the Fe−NO and N−O bond strength sensitivities are dominated by FeNO electron density in either the HOMO or the HOMO−1, which is $\pi$-antibonding throughout the entire Fe−N−O triatomic unit.

## Methods

The theoretical techniques used in this study are based on the density functional theory of Hohenberg, Kohn, and Sham.[31,32] The accurate computation of geometries, vibrational frequencies, and energies of transition metal containing systems is known to require extensive electron correlation techniques. The DFT methods, which incorporate nonlocal exchange and correlation functionals, have demonstrated the ability to account for much of this electron correlation.[33,34] Moreover, DFT methods are very promising for the study of large systems of biochemical interest, including porphyrins, since electron correlation effects can be included at a fraction of the computational cost of traditional ab initio methods.[35−37]

All electronic structure calculations were performed using the hybrid exchange-correlation functional B3LYP, as implemented in Gaussian 98.[38] This functional is Becke's three-parameter exchange functional, in conjunction with the nonlocal correlation functional of Lee, Yang, and Parr.[39] The

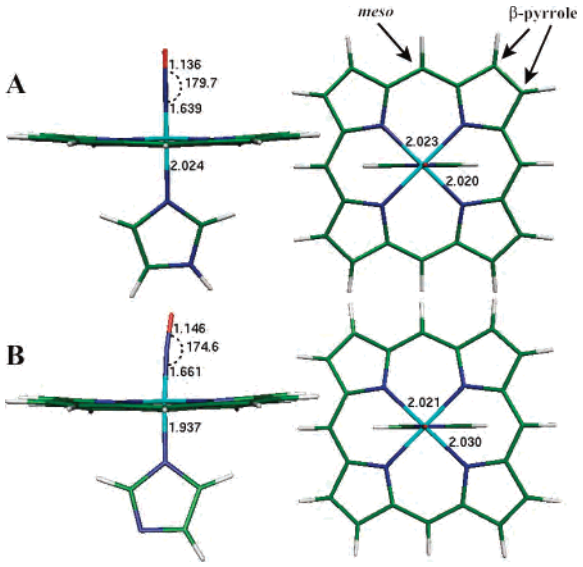


**Figure 2.** Side and top views of six-coordinate {FeNO}$^6$ porphyrinate models. (A) [Fe(P)(ImH)NO]$^+$ and (B) [Fe(P)(Im)NO]. Parameters shown are those of the B3LYP/6-31G(d) optimized structures.

(30) Rich, A. M.; Ellis, P. J.; Tennant, L.; Wright, P. E.; Armstrong, R. S.; Lay, P. A. *Biochemistry* **1999**, *38*, 16491−16499.
(31) (a) Hohenberg, P.; Kohn, W. *Phys. Rev. B* **1964**, *136*, 864−871. (b) Kohn, W.; Sham, L. *Phys. Rev. A* **1965**, *140*, 1133−1138.
(32) Parr, R. G.; Yang, W. *Density-Functional Theory of Atoms and Molecules*; Oxford University Press: New York, 1989.
(33) Ziegler, T. *Chem. Rev.* **1991**, *91*, 651−657.
(34) Siegbahn, P. E. M.; Blomberg, M. R. A. *Annu. Rev. Phys. Chem.* **1999**, *50*, 221−249.
(35) For a review of DFT calculations on porphyrin systems see: Ghosh, A. In *The Porphyrin Handbook*; Kadish, K. M., Smith, K. M., Guilard, R., Eds.; Academic Press: New York, 2000; Vol. 7, pp 1−38.
(36) Liu, Y.-P. *J. Chem. Inf. Comput. Sci.* **2001**, *41*, 22−29.
(37) Rovira, C.; Kunc, K.; Hutter, J.; Ballone, P.; Parrinello, M. *J. Phys. Chem. A* **1997**, *101*, 8914−8925.
(38) Frisch, M. J.; Trucks, G. W.; Schlegel, H. B.; Scuseria, G. E.; Robb, M. A.; Cheeseman, J. R.; Zakrzewski, V. G.; Montgomery, J. A., Jr.; Stratmann, R. E.; Burant, J. C.; Dapprich, S.; Millam, J. M.; Daniels, A. D.; Kudin, K. N.; Strain, M. C.; Farkas, O.; Tomasi, J.; Barone, V.; Cossi, M.; Cammi, R.; Mennucci, B.; Pomelli, C.; Adamo, C.; Clifford, S.; Ochterski, J.; Petersson, G. A.; Ayala, P. Y.; Cui, Q.; Morokuma, K.; Rega, N.; Salvador, P.; Dannenberg, J. J.; Malick, D. K.; Rabuck, A. D.; Raghavachari, K.; Foresman, J. B.; Cioslowski, J.; Ortiz, J. V.; Baboul, A. G.; Stefanov, B. B.; Liu, G.; Liashenko, A.; Piskorz, P.; Komaromi, I.; Gomperts, R.; Martin, R. L.; Fox, D. J.; Keith, T.; Al-Laham, M. A.; Peng, C. Y.; Nanayakkara, A.; Challacombe, M.; Gill, P. M. W.; Johnson, B.; Chen, W.; Wong, M. W.; Andres, J. L.; Gonzalez, C.; Head-Gordon, M.; Replogle, E. S.; Pople, J. A. *Gaussian 98*, revision A.11.4; Gaussian, Inc.: Pittsburgh, PA, 2002.
(39) (a) Becke, A. D. *J. Chem. Phys.* **1993**, *98*, 5648−5652. (b) Lee, C. T.; Yang, W. T.; Parr, R. G. *Phys. Rev. B* **1988**, *37*, 785−789. (c) Stephens, P. J.; Devlin, F. J.; Chablowski, C. F.; Frisch, M. J. *J. Phys. Chem.* **1994**, *98*, 11623−11627.

DFT methods and the B3LYP approach in particular have been used on many other Fe and Fe-porphyrin systems, and they appear to give reasonable results.[40,41] The basis set used consists of the 6-31G(d) set for all atoms except Fe which is the all electron basis set of Wachters and Hay using the scaling factors of Raghavachari and Trucks and including diffuse functions (6-311+G).[42] An ultrafine integration grid was used in all calculations to ensure numerical accuracy. Additionally, we use the linear scaling factor of 0.961 for the computation of harmonic vibrational frequencies, as reported for the B3LYP/6-31G(d) method.[43]

All calculations were performed under $C_s$ symmetry constraints unless otherwise stated. The plane of symmetry includes the Fe−N−O unit and bisects adjacent Fe−N(pyrrole) (Fe−$N_p$) bonds with the trans ImH or $Im^-$ ligand parallel to this plane. A geometry very close to this orientation has been reported in the high-resolution X-ray structure of NP4−NO (PDB code: 1KOI).[24] All results are obtained from the all-electron restricted Kohn−Sham calculations for the systems of singlet spin multiplicity. Experimental results indicate a low spin, diamagnetic ground state for the {FeNO}$^6$ heme proteins and model complexes containing a trans ImH or $Im^-$ ligand.[7,23,44]

The forthcoming discussion involves significant comparison of six-coordinate {FeNO}$^6$ porphyrins with their six-coordinate [$Fe^{II}$CO] analogues. This comparison is appropriate and applicable because {FeNO}$^6$ and [$Fe^{II}$CO] porphyrinates are isoelectronic, and their Fe−X−O geometries both tend toward linearity. Additionally, the [$Fe^{II}$CO] systems have been throughly studied, both experimentally and theoretically, and their inverse $\nu_{Fe-CO}$ versus $\nu_{C-O}$ correlation is well established. The DFT calculations reported here for the [$Fe^{II}$CO] systems were carried out in the manner as described for the {FeNO}$^6$ complexes.

## Results

The results of the DFT calculations for the [Fe(P)(ImH)NO]$^+$ and [Fe(P)(Im)NO] complexes are shown in Table 1. This table contains relevant bond lengths, bond angles, and the scaled ($\times$0.961) harmonic vibrational frequencies associated with these geometries. Additionally, experimental parameters for relevant {FeNO}$^6$ heme proteins and model complexes are included in Table 1 for comparison.

**1. Comparison of Axial Ligand Bonding in [Fe(P)(ImH)NO]$^+$ and [Fe(P)(Im)NO].** The DFT-optimized structure of [Fe(P)(ImH)NO]$^+$ agrees well with reported structures of six-coordinate {FeNO}$^6$ model complexes containing an ImH or other nitrogenous base trans to NO. Although the experimental {FeNO}$^6$ heme protein data are more varied, the range of calculated bonding parameters for [Fe(P)(ImH)NO]$^+$ and [Fe(P)(Im)NO] agrees well with those reported for the proteins (Table 1). There is a significant difference between the calculated Fe−NO bond lengths in [Fe(P)(Im)NO] ($R_{Fe-NO}$ = 1.661 Å) and [Fe(P)(ImH)NO]$^+$ ($R_{Fe-NO}$ = 1.639 Å), as illustrated in Figure 2. For these structures, the calculated Fe−N($Im^-$) bond is substantially shorter than the Fe−N(ImH) bond ($R_{Fe-N}$ = 1.937 and 2.024 Å, respectively), which suggests that the Fe−NO and Fe−$N_{proximal}$ bond strengths are inversely correlated. The DFT calculations also indicate similar and relatively short N−O bond lengths in the [Fe(P)(ImH)NO]$^+$ and [Fe(P)(Im)NO] complexes with distances of 1.136 and 1.146 Å, respectively. In fact, theory and experiment are consistent in showing that $R_{N-O}$ is shorter in six-coordinate {FeNO}$^6$ porphyrinates with proximal nitrogenous ligands than in free NO ($R_{N-O}$ = 1.151 Å (experimental);[47] 1.159 Å (DFT)). This effect is also indicated by higher $\nu_{N-O}$ frequencies in these {FeNO}$^6$ systems relative to free NO ($\nu_{N-O}$ = 1877 $cm^{-1}$ (experimental);[47] 1913 $cm^{-1}$ (DFT)). Finally, the calculations indicate that the Fe−N−O moiety is nearly linear for [Fe(P)(ImH)NO]$^+$ with ∠FeNO = 179.7°, while FeNO is slightly bent in [Fe(P)(Im)NO], wherein ∠FeNO = 174.6°. These angles are well within the range of experimental values, with the exception of the highly bent NP4−NO complex (Table 1).

Effects of basis set size on axial ligand bonding in [Fe(P)(ImH)NO]$^+$ and [Fe(P)(Im)NO] were investigated by increasing our basis set size to 6-311G(2d,p). The bonding parameters from the respective optimized structures are listed in Table 1. The larger basis set has only a small impact on the optimized geometries of these two complexes. The largest discrepancy is the N−O bond length, both of which are shorter by 0.013 Å in the 6-311G(2d,p) optimized structures. All Fe−N bond lengths change by ≤0.006 Å. Wondimagegn et al.[48] have performed a geometry optimization calculation on the [Fe(P)(ImH)NO]$^+$ system, using the PW91 exchange-correlation functional and a triple-$\zeta$ plus polarization quality basis set, and obtained FeNO bonding parameters of $R_{Fe-NO}$ = 1.639 Å, $R_{N-O}$ = 1.149 Å, and ∠FeNO = 179.8°, all similar to the results of the B3LYP calculations reported here. Since the effect of the larger basis sets on calculated bond lengths is small and since the differences do not change the correlations between Fe−NO and N−O bond strengths (vide infra), we have used the 6-31G(d) basis set throughout this study.

The Fe−NO and N−O vibrational frequency differences between the [Fe(P)(ImH)NO]$^+$ and [Fe(P)(Im)NO] complexes are consistent with the differences between the bond lengths, with $\nu_{Fe-NO}$ and $\nu_{N-O}$ frequencies of the former complex being greater than those of the latter. The DFT $\nu_{N-O}$


(40) Salomon, O.; Reiher, M.; Hess, B. A. *J. Chem. Phys.* **2002**, *117*, 4729−4737.
(41) Zhang, Y.; Mao, J.; Godbout, N.; Oldfield, E. *J. Am. Chem. Soc.* **2002**, *124*, 13921−13930.
(42) (a) Raghavachari, K.; Trucks, G. W. *J. Chem. Phys.* **1989**, *91*, 1062−1065. (b) Wachters, A. J. H. *J. Chem. Phys.* **1970**, *52*, 1033−1036. (c) Hay, P. J. *J. Chem. Phys.* **1977**, *66*, 4377−4384.
(43) Foresman, J. B.; Frisch, A. *Exploring Chemistry with Electronic Structure Methods*, 2nd ed.; Gaussian, Inc.: Pittsburgh, PA, 1996.
(44) Hori, H.; Ikeda-Saito, M.; Lang, G.; Yonetani, T. *J. Biol. Chem.* **1990**, *265*, 15028−15033.
(45) Ellison, M. K.; Scheidt, W. R. *J. Am. Chem. Soc.* **1999**, *121*, 5210−5219.
(46) Ellison, M. K.; Schulz, C. E.; Scheidt, W. R. *J. Am. Chem. Soc.* **2002**, *124*, 13833−13841.
(47) *NIST-JANAF Thermochemical Tables*, 4th ed.; Chase, M. W., Jr., Ed.; Journal of Physical and Chemical Reference Data Monograph No. 9.; American Chemical Society: Washington, DC, 1998.
(48) Wondimagegn, T.; Ghosh, A. *J. Am. Chem. Soc.* **2001**, *123*, 5680−5683.

**Table 1.** Six-Coordinate {FeNO}$^6$ Theoretical and Experimental Bond Lengths, Bond Angles, and Vibrational Stretching Frequencies[a]

| system | $R_{Fe-NO}$ | $R_{N-O}$ | ∠FeNO | $R_{Fe-N(L)}$ | $R_{Fe-Np}$ | $\nu_{Fe-NO}$ | $\nu_{N-O}$ | $\delta_{Fe-NO}$ | (references) comments |
|---|---|---|---|---|---|---|---|---|---|
| $[Fe(P)(ImH)NO]^+$ (imidazole) | 1.639 | 1.136 | 179.7 | 2.024 | 2.020, 2.023 | 630 | 1981 | 597, 588 | DFT, 6-31G(d) |
| $[Fe(P)(ImH)NO]^+$ | 1.644 | 1.122 | 179.9 | 2.029 | 2.017, 2.019 | nc | nc | nc | DFT, 6-311G(2d,p) |
| [Fe(P)(Im)NO] (imidazolate) | 1.661 | 1.146 | 174.6 | 1.937 | 2.021, 2.030 | 590 | 1924 | 581, 612 | DFT, 6-31G(d) |
| [Fe(P)(Im)NO] | 1.663 | 1.132 | 176.7 | 1.944 | 2.020, 2.024 | nc | nc | nc | DFT, 6-311G(2d,p) |
| $[Fe(P)NO]^+$ (5-coordinate) | 1.614 | 1.145 | 180.0 | - - | 2.006 | 682 | 1932 | | (9) |
| Proteins and Complexes | | | | | | | | | |
| $[Fe(OEP)(1\text{-}MeIm)NO]^+$ | 1.646 | 1.135 | 177.3 | 1.989 | 2.003 | | 1921 | | (45) |
| $[Fe(OEP)(Pyrazole)NO]^+$ | 1.627 | 1.141 | 176.9 | 1.988 | 2.004 | | 1909 | | (45) |
| $[Fe(OETPP)(1\text{-}MeIm)NO]^+$ | 1.650 | 1.130 | 177.0 | 1.983 | 1.990 | | 1871 | | (46) |
| $[Fe(OEP)(Indazole)NO]^+$ | 1.632 | 1.136 | 177.6 | 2.010 | 1.996 | | 1914 | | (45) |
| NP4(III)-NO | 1.66 | 1.08 | 156.0 | 2.013 | 1.99, 2.00 | | | | (24) nitrophorin4, PDB: 1KOI |
| Mb(III)-NO | 1.68 | 1.13 | 180 | 2.04 | 2.00 | | | | (25) myoglobin (MS-XAFS) |
| Lb(III)-NO | 1.68 | 1.12 | 173 | 1.89 | 2.00 | | | | (30) leghemoglobin *a* (MS-XAFS) |
| NP1(III)-NO | | | | | | 591 | 1917, 1904 | 578 | (21) nitrophorin 1 from *R. prolixus* saliva |
| hHO-1 | | | | | | 596 | 1918 | 588 | (19) human heme oxygenase-1 |
| metMb(III)-NO | | | | | | 595 | 1927, 1922 | 573 | (14, 16, 17) myoglobin |
| HbA(III)-NO | | | | | | 594 | 1925 | 574 | (14, 15) hemoglobin A |
| HRP(III)-NO | | | | | | 604 | 1903 | 574 | (14, 16) horseradish peroxidase |
| NOR(III)-NO | | | | | | 594 | 1904 | | (20) bacterial nitric oxide reductase |
| HbN(III)-NO | | | | | | 591 | 1914 | | (18) HbN, from *M. tuberculosis* |
| HbN(III)-NO Y33F | | | | | | 592 | 1908 | | (18) HbN mutant |
| Substituted Models (Imidazole) | | | | | | | | | |
| $[Fe(P\text{-}\beta\text{-}F_8)(ImH)NO]^+$ | 1.645 | 1.134 | 179.7 | 2.023 | 2.017, 2.019 | 619 | 1987 | 589, 597 | |
| $[Fe(P\text{-}\beta\text{-}(NH_2)_4)(ImH)NO]^+$ | 1.634 | 1.138 | 179.7 | 2.025 | 2.020, 2.025 | 636 | 1971 | 587, 593 | |
| $[Fe(P\text{-}meso\text{-}F_4)(ImH)NO]^+$ | 1.642 | 1.134 | 179.9 | 2.026 | 2.019, 2.020 | 621 | 1986 | 570, 578 | |
| $[Fe(P\text{-}meso\text{-}(NH_2))(ImH)NO]^+$ | 1.639 | 1.137 | 176.5 | 2.025 | 2.013, 2.022 | 620 | 1973 | 579 | |
| $[Fe(P\text{-}meso\text{-}(NH_2)_2)(ImH)NO]^+$ | 1.659 | 1.140 | 171.2 | 2.016 | 1.999, 2.030 | 507 | 1947 | 555, 567 | |
| $[Fe(P\text{-}meso\text{-}((NH_2)_2,Cl)(ImH)NO]^+$ | 1.672 | 1.141 | 167.8 | 2.009 | 1.994, 2.028 | 501 | 1934 | 547, 570 | |
| $[Fe(P\text{-}meso\text{-}((NH_2)_2,Cl_2)(ImH)NO]^+$ | 1.793 | 1.154 | 144.0 | 1.998 | 1.982, 2.019 | nc | nc | nc | |
| $[Fe(P\text{-}meso\text{-}((NH_2)_2,F)(ImH)NO]^+$ | 1.812 | 1.158 | 141.1 | 1.998 | 1.988, 2.029 | 382 | 1775 | 445, 452 | |
| $[Fe(P\text{-}meso\text{-}((NH_2)_2,F_2)(ImH)NO]^+$ | 1.845 | 1.162 | 137.2 | 2.004 | 1.991, 2.022 | nc | nc | nc | |
| $[Fe(P\text{-}meso\text{-}(NH_2)_3)(ImH)NO]^+$ | 1.860 | 1.170 | 132.3 | 2.018 | 1.982, 2.013 | 379 | 1695 | | |
| $[Fe(P\text{-}meso\text{-}(NH_2,F)(ImH)NO]^+$ | 1.642 | 1.137 | 175.8 | 2.024 | 2.008, 2.026 | 602 | 1971 | 573, 580 | |
| $[Fe(P\text{-}meso\text{-}(NH_2,F_2)(ImH)NO]^+$ | 1.654 | 1.138 | 172.0 | 2.016 | 2.005, 2.028 | 561 | 1960 | 570, 570 | |
| $[Fe(P\text{-}meso\text{-}(NH_2,F_3)(ImH)NO]^+$ | 1.676 | 1.140 | 167.1 | 2.006 | 1.997, 2.035 | 546 | 1936 | 542, 568 | 6-31G(d) |
| $[Fe(P\text{-}meso\text{-}(NH_2,F_3)(ImH)NO]^+$ | 1.662 | 1.125 | 171.8 | 2.023 | 1.998, 2.026 | nc | nc | nc | 6-311G(2d,p) |
| Substituted Models (Imidazolate) | | | | | | | | | |
| $[Fe(P\text{-}\beta\text{-}F_8)(Im)NO]$ | 1.669 | 1.144 | 174.6 | 1.930 | 2.019, 2.027 | 577 | 1928 | 572, 609 | |
| $[Fe(P\text{-}\beta\text{-}(NH_2)_4)(Im)NO]$ | 1.656 | 1.145 | 176.3 | 1.943 | 2.027, 2.027 | 599 | 1929 | 587, 611 | |
| $[Fe(P\text{-}meso\text{-}F_4)(Im)NO]$ | 1.680 | 1.146 | 165.8 | 1.930 | 2.009, 2.036 | 558 | 1909 | 561, 579 | |
| $[Fe(P\text{-}meso\text{-}(NH_2))(Im)NO]$ | 1.665 | 1.146 | 170.4 | 1.937 | 2.018, 2.036 | 577 | 1918 | 576, 606 | |
| $[Fe(P\text{-}meso\text{-}(NH_2)_2)(Im)NO]$ | 1.679 | 1.148 | 164.6 | 1.938 | 1.996, 2.027 | 533 | 1896 | 573, 578 | |
| $[Fe(P\text{-}meso\text{-}((NH_2)_2,F)(Im)NO]$ | 1.703 | 1.152 | 158.0 | 1.937 | 1.986, 2.032 | 540 | 1863 | 549, 557 | |
| $[Fe(P\text{-}meso\text{-}(NH_2,F)_2(Im)NO]$ | 1.733 | 1.155 | 151.8 | 1.937 | 1.985, 2.028 | 516 | 1826 | 507, 535 | 6-31G(d) |
| $[Fe(P\text{-}meso\text{-}(NH_2,F)_2(Im)NO]$ | 1.707 | 1.138 | 158.5 | 1.943 | 1.986, 2.024 | nc | nc | nc | 6-311G(2d,p) |
| $[Fe(P\text{-}meso\text{-}(NH_2)_3)(Im)NO]$ | 1.761 | 1.163 | 144.9 | 1.948 | 1.973, 2.022 | 492 | 1768 | 499 | |

[a] All theoretical parameters are from B3LYP/6-31G(d) calculations, and calculated frequencies are scaled by 0.961. Bond lengths in angstroms (Å), bond angles in degrees (°), frequencies in wavenumbers ($cm^{-1}$), L = trans ligand, $N_p$ = pyrrole nitrogen atom. Abbreviations: P, porphyrinate (dianion of porphine); Por, generalized porphyrinate; ImH, imidazole; $Im^-$, imidazolate; OEP, octaethylporphyrinate; TPP, tetrakis(5, 10, 15, 20)phenylporphyrinate; nc, not calculated.

frequencies are 1981 and 1924 $cm^{-1}$ for $[Fe(P)(ImH)NO]^+$ and [Fe(P)(Im)NO], respectively, with corresponding $\nu_{Fe-NO}$ frequencies of 630 and 590 $cm^{-1}$. The experimental $\nu_{Fe-NO}$ frequencies (591−604 $cm^{-1}$) for {FeNO}$^6$ heme proteins and model complexes fall between those calculated for $[Fe(P)(ImH)NO]^+$ and [Fe(P)(Im)NO] and tend toward the $Im^-$ end of the calculated range. The experimental $\nu_{N-O}$ values (1871−1927 $cm^{-1}$) also tend toward the $Im^-$ end of the calculated $\nu_{N-O}$ range. This tendency toward the FeNO frequencies of [Fe(P)(Im)NO] is not particularly surprising, as heme proteins and model complexes exhibit a range of H-bond strengths between the proximal imidazole and H-bond acceptors, with totally non-H-bonded ImH being relatively rare. Moreover, the hemes in proteins contain substituted porphyrinate and experimental FeNO bonding parameters are obtained from solution or crystal structures where interactions with solvent are plentiful. Since the calculated frequencies were obtained for isolated unsubstituted porphine complexes in the gas phase, small differences in vibrational frequencies are not unexpected. Considering these caveats, the agreement between the calculated and experimental parameters is quite good.

**2. Substituted Models.** With a starting model in hand that accurately mimics experimental structures and spectroscopic properties of six-coordinate-{FeNO}$^6$ porphyrinates, we set out to establish the basis of the relationship between the sensitivities of the Fe−NO and N−O bond strengths to changes in structure and environment. While the hemes in many proteins have similar peripheral substitution patterns, their distal and proximal environments differ in amino acid composition and in the number, types, and strengths of electrostatic interactions. Such variations in the electrostatic environments are difficult to model systematically, as choice and design of distal electrostatic interactions with axial ligands has high dimensionality.[49] For five-coordinate CO, NO, and $O_2$ adducts of $Fe^{II}$(Por) and for six-coordinate [$Fe^{II}$(Por)(ImH)CO] complexes, it has been shown experimentally that porphyrin peripheral substitutions produce inverse vibrational frequency correlations. In this regard, the FeXO moieties respond in much the same way as they would if the molecule were subjected to a series of distal electrostatic fields, such as those experienced across a series of protein environments.[10,11] Therefore, to induce shifts in the $\nu_{Fe-NO}$ and $\nu_{N-O}$ frequencies of our model systems, we have exploited these cis or equatorial effects on FeXO bonding by modifying the structural and electronic properties of the porphine periphery with $-NH_2$, $-F$, and $-Cl$ substituents in $\beta$-pyrrole and meso positions. Using this approach, full geometry optimizations and frequency calculations can be performed without imposing arbitrary distance and/or geometry constraints. The Fe−N−O bond lengths, angles, and vibrational frequencies calculated using this approach are listed in Table 1. The analogous Fe−C−O parameters for the isoelectronic [$Fe^{II}$(Por)(ImH)CO] and [$Fe^{II}$(Por)(Im)CO]$^-$ are listed in Table S1.

**2a. [Fe(Por)(ImH)NO]$^+$; FeNO Geometry and Vibrational Frequencies.** From Table 1, it is clear that modifications of the porphyrin periphery have a profound influence on the Fe−N−O geometry. This is especially true for variations in meso substituents. Not only do the Fe−NO and N−O bond distances change significantly, but the Fe−N−O angle does as well. The corresponding vibrational frequency correlation plot constructed from the data in Table 1 is shown in Figure 3.[50] Overall, it is clear from this figure that factors affecting the bonding in the FeNO triatomic unit either increase or decrease both $\nu_{Fe-NO}$ and $\nu_{N-O}$. That is, our theoretical model predicts a *direct* correlation between $\nu_{Fe-NO}$ and $\nu_{N-O}$ frequencies for the [Fe(Por)(ImH)NO]$^+$ systems. Analogous calculations performed on the isoelectronic [$Fe^{II}$-(Por)(ImH)CO] complexes show the expected *inverse* correlation betwen $\nu_{Fe-CO}$ and $\nu_{C-O}$ that is uniformly observed for heme proteins and model complexes. This result is shown in the inset of Figure 3. Furthermore, the direct $\nu_{Fe-NO}$ versus $\nu_{N-O}$ correlation is extensive, spanning a $\Delta\nu_{Fe-NO}$ range of 257 cm$^{-1}$ (379−636 cm$^{-1}$) and a $\Delta\nu_{N-O}$ range of 292 cm$^{-1}$ (1695−1987 cm$^{-1}$). The analogous calculations for the [$Fe^{II}$-(Por)(ImH)CO] complexes give values spanning a small fraction of this range, 19 cm$^{-1}$ for $\Delta\nu_{Fe-CO}$ and 23 cm$^{-1}$ for $\Delta\nu_{C-O}$.

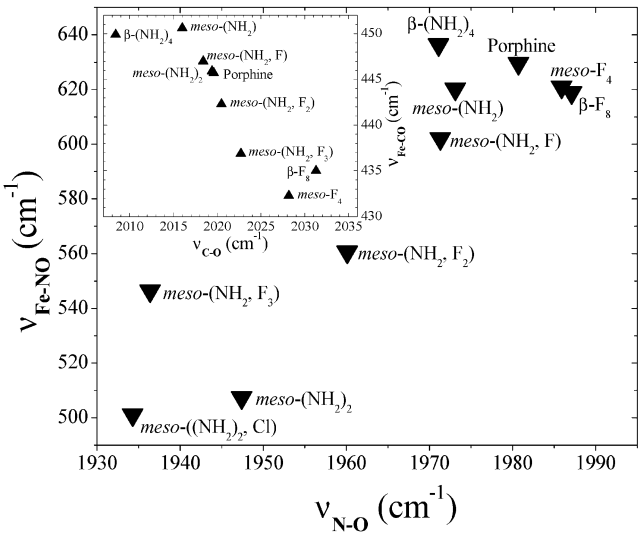


**Figure 3.** Correlation between $\nu_{Fe-NO}$ and $\nu_{N-O}$ frequencies for six-coordinate [Fe(Por)(ImH)NO]$^+$ complexes as calculated at the B3LYP/6-31G(d) level of theory. Inset, [Fe(Por)(ImH)CO] complexes.

Systematic variation in ∠FeNO for these complexes raises the question of whether the vibrational frequencies provide an accurate picture of the bonding interactions occurring within the FeNO unit. For the fully optimized [$Fe^{II}$(Por)-(ImH)CO] systems, the FeCO moiety is always linear (∠FeCO > 179°). However, the data in Table 1 reveal that ∠FeNO tracks the FeNO vibrational frequencies for [Fe-(Por)(ImH)NO]$^+$ complexes having 132.3° ≤ ∠FeNO ≤ 179.7°. This bending induces changes in the contributions of Fe−NO stretching and Fe−N−O bending coordinates to the normal modes involving FeNO motion. Consequently, it could complicate the gauging of Fe−NO and N−O bond strengths based on vibrational frequencies. To address this issue, a correlation between the calculated Fe−NO and N−O bond lengths was plotted and is shown in Figure 4. This figure unambiguously shows that $R_{Fe-NO}$ and $R_{N-O}$ either increase or decrease in concert, consistent with the vibrational data. Moreover, and consistent with the ranges of the vibrational frequencies, the bond length ranges are substantial, with $\Delta R_{Fe-NO}$ spanning 0.226 Å (1.634−1.860 Å) and $\Delta R_{N-O}$ = 0.036 Å (1.134−1.170 Å). The corresponding values for [$Fe^{II}$(Por)(ImH)CO] are $\Delta R_{Fe-CO}$ = 0.017 Å and $\Delta R_{C-O}$ = 0.004 Å, which are much smaller than the {FeNO}$^6$ values and, of course, $R_{Fe-CO}$ and $R_{C-O}$ are inversely correlated, as shown in the inset of Figure 4. Although examination of the vibrational eigenvectors reveals that mixing of internal FeNO coordinates does occur, the clear bond length correlation indicates that the direct frequency

(49) Frazen, S. *J. Am. Chem. Soc.* **2002**, *124*, 13271−13281.

(50) A note of clarification, The $Fe^{III}$NO data in Figures 3 and 4 do not contain the entire data set from Table 1. The reason for this is that there is a very large gap between the data shown and the remaining four data points. However, a direct correlation is still observed for all of the data points. Moreover, the remaining data points correspond to complexes in which ∠FeNO < 144°. A previous study[51] on $Fe^{III}$NO thiolate systems shows that the singlet electronic state is the ground state for systems in which ∠Fe−N−O ≳ 140°. For ∠Fe−N−O ≲ 135°, the triplet and quintet states become lower in energy. We have not performed calculations on states of higher spin multiplicity for any of our systems as the parameters from the highly bent complexes are not necessary to explain the correlations between indicators of Fe−XO and X−O bond strengths.

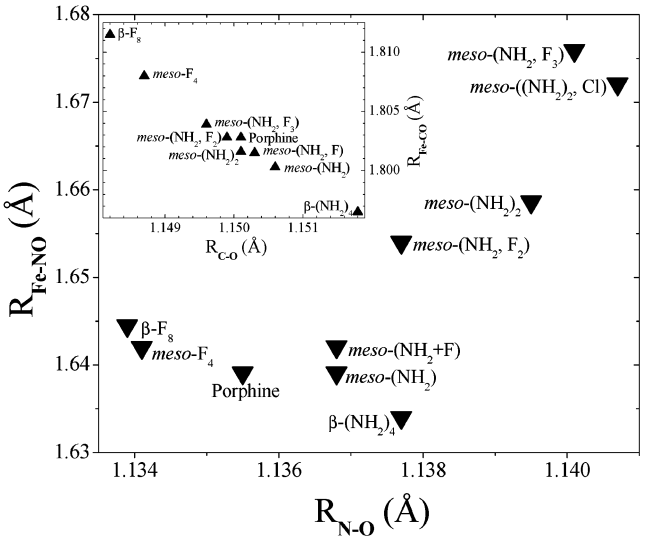


**Figure 4.** Correlation between Fe−NO and N−O bond lengths for six-coordinate [Fe(Por)(ImH)NO]$^+$ complexes at the B3LYP/6-31G(d) level of theory. Inset, [Fe(Por)(ImH)CO] complexes.

correlation is not attributable to ∠FeNO-dependent changes in normal mode compositions.

In the initial stages of performing DFT calculations on substituted [Fe(Por)(ImH)NO]$^+$ complexes, it became apparent that choice of peripheral substitutents could have a large effect on ∠FeNO. Therefore, we have attempted to quantify the energetics of Fe−N−O bending by performing a series of constrained geometry optimizations holding only ∠FeNO fixed at 5° increments from 179.7° to 155.0°. This set of calculations can be viewed as modeling of FeNO bending in response to distal steric interactions that induce minimal electrostatic polarization within {FeNO}$^6$. The results are listed in Table 2 with the corresponding bond length correlation plot shown in Figure 5. Two interesting properties of the {FeNO}$^6$ moieties are revealed by these calculations. First, {FeNO}$^6$ is quite flexible, requiring very little energy to perturb its geometry. In fact, bending the linear FeNO unit 15° (to 165.0°) requires less than 1 kcal/mol, while a bend of 25° (to 155°) requires less than 3 kcal/mol ($RT$ = 0.6 kcal/mol at 300 K). This energy cost is consistent with that calculated for six-coordinate [Fe$^{II}$CO] porphyrinate having a proximal ImH ligand.[52] {FeNO}$^6$ structures having ∠FeNO of this magnitude have been observed experimentally in the six-coordinate NP4−NO, which contains a proximal His ligand,[24] and in a porphyrin model complex containing an axial *p*-fluorophenyl ligand trans to NO.[53] Second, Figure 5 shows that $R_{Fe-NO}$ and $R_{N-O}$ are *directly* correlated. That is, bending the FeNO unit to 155.0° increases $R_{Fe-NO}$ by 0.045 Å and $R_{N-O}$ by 0.004 Å. Because the vibrational frequencies calculated for nonequilibrium geometries are not invariant with respect to translation and rotation, they are not reported here. Nevertheless, the bond length correlation suggests that the cause and effect relationship between Fe−N−O bond strengths and ∠FeNO is bidirectional.

**2b. [Fe(Por)(Im)NO]; FeNO Geometry and Vibrational Frequencies.** From Table 1, it is clear that modification of the porphyrin periphery also has a significant influence on the FeNO geometry of the corresponding Im$^-$-bound systems. However, the overall influence is less for the Im$^-$ complexes than for their ImH-bound counterparts. This is first evidenced by the smaller sensitivity of ∠FeNO to substituent effects in the Im$^-$ complexes (∠FeNO = 174.6−144.9° for Im$^-$; ∠FeNO = 179.7−132.3° for ImH). Figure 6 shows the vibrational frequency correlation plot constructed from the data on Im$^-$ complexes in Table 1. This figure clearly illustrates that factors affecting the FeNO triatomic unit either increase or decrease the frequencies of both $\nu_{Fe-NO}$ and $\nu_{N-O}$. Hence, our theoretical model also predicts a *direct* vibrational stretching frequency correlation for the series of [Fe(Por)(Im)NO] complexes. This correlation spans $\Delta\nu_{Fe-NO}$ and $\Delta\nu_{N-O}$ ranges of 107 cm$^{-1}$ (492−599 cm$^{-1}$) and 161 cm$^{-1}$ (1768−1929 cm$^{-1}$), respectively. Although these ranges are smaller than those for the ImH complexes, they are substantially larger than the corresponding ranges for the isoelectronic [Fe$^{II}$(Por)(Im)CO]$^-$ complexes ($\Delta\nu_{Fe-CO}$ = 19 cm$^{-1}$ and $\Delta\nu_{C-O}$ = 15 cm$^{-1}$). Analogous calculations performed on the isoelectronic [Fe$^{II}$(Por)(Im)CO]$^-$ systems once again show the expected *inverse* correlation between $\nu_{Fe-CO}$ and $\nu_{C-O}$ frequencies, as shown in the inset of Figure 6. Consistent with the vibrational frequencies, Figure 7 shows that $R_{Fe-NO}$ and $R_{N-O}$ are also directly correlated. Moreover, and consistent with the range in vibrational frequencies, the range of bond lengths is large with $\Delta R_{Fe-NO}$ spanning 0.105 Å (1.656−1.761 Å) and $\Delta R_{N-O}$ = 0.018 Å (1.145−1.163 Å). The corresponding ranges for the [Fe$^{II}$(Por)(Im)CO]$^-$ complexes are $\Delta R_{Fe-CO}$ = 0.014 Å and $\Delta R_{C-O}$ = 0.002 Å, about one-eighth of the {FeNO}$^6$ ranges with $R_{Fe-CO}$ and $R_{C-O}$ showing the expected inverse correlation (inset of Figure 7).

Although large variations in ∠FeNO (down to 144.9° for P-*meso*-(NH$_2$)$_3$) in the [Fe(Por)(Im)NO] complexes could complicate interpretation of FeNO frequencies because of angle-dependent changes in normal mode composition, the correlation between the Fe−NO and N−O bond lengths shown in Figure 7 is a clear indication that systematic variations in normal mode composition do not play a dominant role in either the sign or magnitude of the vibrational frequency correlation. However, these variations probably influence the shape of the vibrational frequency correlation; Figure 6 does exhibit noticeable curvature. The decrease in slope of the correlation with decreasing ∠FeNO is consistent with the Fe−NO stretching potential becoming increasingly distributed across other normal modes as the equilibrium FeNO geometry becomes more bent. Interestingly, the vibrational frequency correlation for the ImH complexes (Figure 3) does not appear to be curved. The curvature in Figure 6 may be a result of changes in the normal mode compositions in the Im$^-$ complexes due to weaker Fe−N−O bonding.

(51) Scherlis, D. A.; Cymeryng, C. B.; Estrin, D. A. *Inorg. Chem.* **2000**, *39*, 2352−2359.
(52) Ghosh, A.; Bocian, D. F *J. Phys. Chem.* **1996**, *100*, 6363−6366.
(53) Richter-Addo, G. B.; Wheeler, R. A.; Hixson, L. A.; Chen, L.; Khan, M. A.; Ellison, M. K.; Schulz, C. E.; Scheidt, W. R. *J. Am. Chem. Soc.* **2001**, *123*, 6314−6326.

**Table 2.** Theoretical Bond Lengths and Bond Angles from Constrained-Geometry Optimizations of Six-Coordinate [Fe(P)(ImH)NO]$^{+}$ [a]

| system | $R_{Fe-NO}$ | $R_{N-O}$ | ∠FeNO | $R_{Fe-N(ImH)}$ | $R_{Fe-Np}$ | relative energy (kcal/mol) |
|---|---|---|---|---|---|---|
| [Fe(P)(ImH)NO]+ | 1.639 | 1.136 | 179.7 | 2.024 | 2.020, 2.023 | +0.0 |
| ∠Fe−N−O fixed at 175.0 | 1.641 | 1.136 | 175.0 | 2.022 | 2.016, 2.027 | +0.1 |
| ∠Fe−N−O fixed at 170.0 | 1.646 | 1.136 | 170.0 | 2.017 | 2.012, 2.030 | +0.4 |
| ∠Fe−N−O fixed at 165.0 | 1.655 | 1.137 | 165.0 | 2.011 | 2.008, 2.033 | +0.9 |
| ∠Fe−N−O fixed at 160.0 | 1.668 | 1.138 | 160.0 | 2.004 | 2.004, 2.035 | +1.6 |
| ∠Fe−N−O fixed at 155.0 | 1.684 | 1.140 | 155.0 | 1.997 | 2.000, 2.037 | +2.6 |

[a] All parameters are from B3LYP/6-31G(d) calculations. Bond lengths in angstroms (Å), bond angles in degrees (°), $N_p$ = pyrrole nitrogen atom.

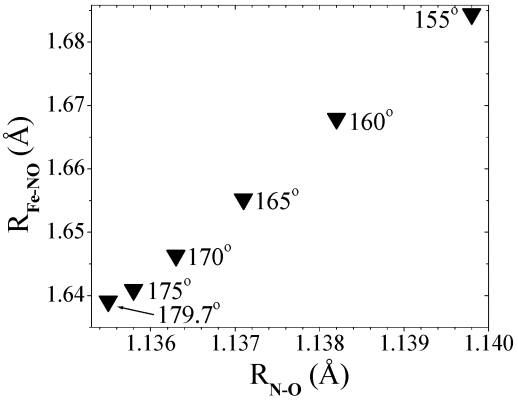


**Figure 5.** Correlation between $R_{Fe-NO}$ and $R_{N-O}$ for the [Fe(P)(ImH)NO]$^{+}$ complex for which ∠FeNO was constrained at the indicated values.

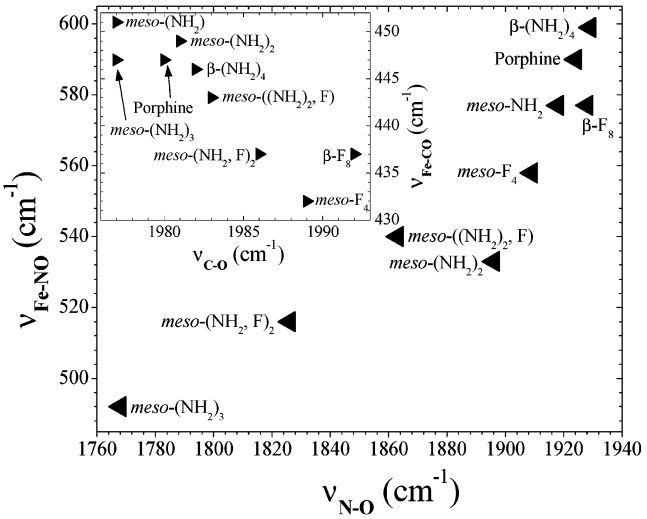


**Figure 6.** Correlation between $\nu_{Fe-NO}$ and $\nu_{N-O}$ frequencies for six-coordinate [Fe(Por)(Im)NO] complexes at the B3LYP/6-31G(d) level of theory. Inset, [Fe(Por)(Im)CO]$^{-}$ complexes.

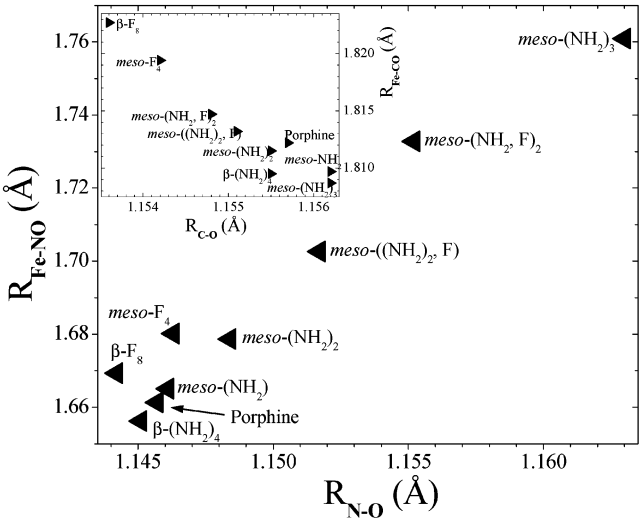


**Figure 7.** Correlation between Fe−NO and N−O bond lengths for six-coordinate [Fe(Por)(Im)NO] complexes at the B3LYP/6-31G(d) level of theory. Inset, [Fe(Por)(Im)CO]$^{-}$ complexes.

## Discussion

Having established that both {FeNO}$^{6}$-imidazole and -imidazolate systems exhibit large *direct* correlations in their Fe−NO and N−O vibrational frequencies and bond lengths, the ensuing discussion aims to establish a cause and effect relationship between systematic changes in FeNO electron densities and the relative sensitivities of Fe−NO and N−O bond strength indicators to changes in structure and environment of {FeNO}$^{6}$ porphyrinates.

**1. Orbitals Responsible for the Direct Correlation between Sensitivities of Fe−NO and N−O Bond Strengths to Structure and Environment. 1a. [Fe(Por)(ImH)NO]$^{+}$.** To understand the vibrational frequency correlations at a fundamental level, it is helpful to examine the Kohn−Sham molecular orbital (MO) representations and identify those to which the bond strength sensitivities can be attributed. Figure 8 shows a collection of MOs for a subset of the [Fe(Por)(ImH)NO]$^{+}$ complexes in Figures 3 and 4 (top) and their isoelectronic [Fe$^{II}$(Por)(ImH)CO] analogues (bottom).[54] They show the Fe−X−O interactions that account for the differences in behavior between these systems. This subset of complexes was chosen because it represents a continuous trend in the bond lengths and vibrational frequencies for both the {FeNO}$^{6}$ and [Fe$^{II}$CO] complexes, which facilitates direct comparison of these isoelectronic systems. The [Fe(Por)(ImH)NO]$^{+}$ complexes in Figure 8 span $\Delta\nu_{Fe-NO}$ and $\nu_{N-O}$ ranges of 84 cm$^{-1}$ (546−630 cm$^{-1}$) and 45 cm$^{-1}$ (1936−1981 cm$^{-1}$), respectively. The corresponding ranges for the [Fe$^{II}$(Por)(ImH)CO] complexes are 10 cm$^{-1}$ (437−447 cm$^{-1}$) and 5 cm$^{-1}$ (2018−2023 cm$^{-1}$).

Figure 8 shows the highest occupied molecular orbitals (HOMOs) for the [Fe(Por)(ImH)NO]$^{+}$ complexes on the top and for the [Fe(Por)(ImH)CO] complexes on the bottom. This set of orbitals show pronounced differences in the FeXO electron density between the respective {FeNO}$^{6}$ and [Fe$^{II}$CO] complexes. Figure 8A shows that the FeXO electron densities in the HOMOs of both [Fe(P)(ImH)NO]$^{+}$ and [Fe(P)(ImH)CO] are very similar. The HOMOs are porphyrin $\pi$ MOs with electron density concentrated on the meso carbon and pyrrole nitrogen atoms. Additionally, these two

(54) All MO figures (isosurfaces) were produced with the program MOLEKEL version 4.2 (http://www.cscs.ch/molekel/). Portman, S.; Lüthi, H. P. *Chimia* **2000**, *54*, 766−770.

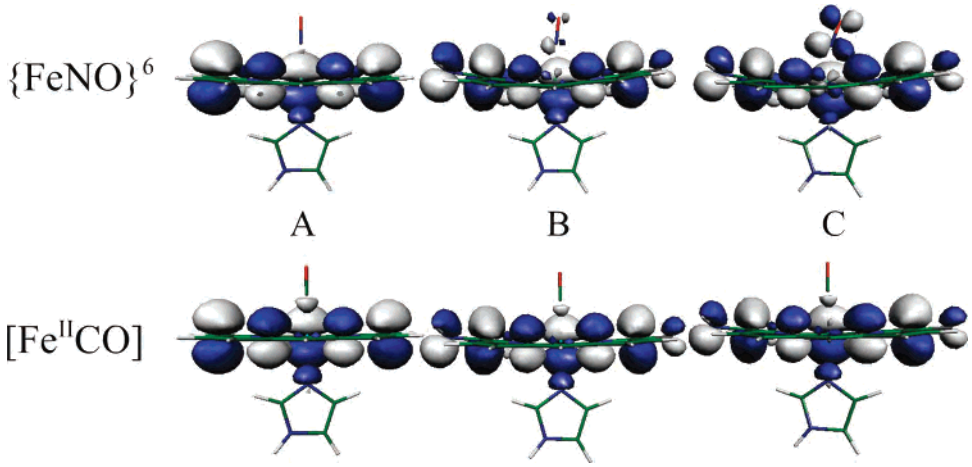


**Figure 8.** HOMOs for ImH complexes. Top, {FeNO}⁶ porphyrinates; bottom, [Fe^IICO] porphyrinates. (A) Porphine, (B) P-*meso*-($NH_2$, F), and (C) P-*meso*-($NH_2$, $F_3$). Electron density at the front edges has been removed to facilitate viewing of the FeNO moiety.

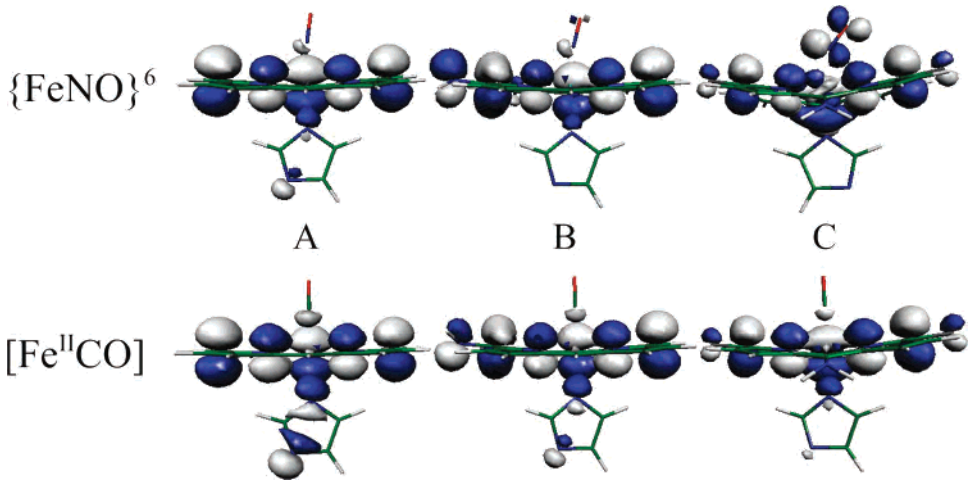


**Figure 9.** HOMOs-1 for $Im^-$ complexes. Top, {FeNO}⁶ porphyrinates; bottom, [Fe^IICO] porphyrinates. (A) Porphine, (B) P-*meso*-($NH_2$), and (C) P-*meso*-($NH_2$, F)$_2$ (HOMO for {FeNO}⁶). Electron density at the front edges has been removed to facilitate viewing of the FeNO moiety.

HOMOs exhibit slight Fe−XO $\sigma$-bonding character with the [Fe^IICO] having the stronger interaction. As peripheral $-NH_2$ and −F substituents are added at the meso positions of the {FeNO}⁶ and [Fe^IICO] complexes, a metamorphosis occurs in the electron density distribution within the HOMOs of the {FeNO}⁶ complexes. The HOMOs of the {FeNO}⁶ porphyrinates undergo a change in FeNO character, from slightly Fe−NO $\sigma$ bonding to strongly $\pi$ antibonding with respect to Fe−N−O. Moreover, Figure 8B,C shows that the HOMOs for [Fe(P-*meso*-($NH_2$, F))(ImH)NO]$^+$ and [Fe(P-*meso*-($NH_2$, $F_3$))(ImH)NO]$^+$ become increasingly $\pi$-antibonding with respect to the Fe−N−O triatomic unit. This increased Fe−N−O $\pi$-antibonding character has the effect of simultaneously diminishing the Fe−NO and N−O bond strengths as electron density is polarized toward the FeNO core by the addition of meso −F and $-NH_2$ substituents. The aforementioned change in FeXO character of the HOMO is not observed in the corresponding [Fe^IICO] complexes. On the other hand, the Fe−CO $\sigma$-bonding character of the [Fe^II(Por)(ImH)CO] HOMOs is virtually unaffected by the same meso substituents.

**1b. [Fe(Por)(Im)NO].** In support of a similar analysis, Figure 9 shows the HOMOs-1 for a series of [Fe(Por)(Im)NO] complexes (top) and their [Fe^II(Por)(Im)CO]$^-$ analogues (bottom). This is the highest occupied MO having significant FeNO electron density; the HOMO is an $Im^-$-based $\pi$ MO that is nonbonding with respect to FeCO and has slight $\pi^*$ character with respect to N−O. The subset of complexes in Figure 9 represents a continuous trend in the bond lengths and vibrational frequencies for $Im^-$ complexes of both the {FeNO}⁶ and [Fe^IICO] porphyrinates. The calculated frequency ranges are $\Delta\nu_{Fe-NO} = 74$ cm$^{-1}$ (516−590 cm$^{-1}$), $\Delta\nu_{N-O} = 98$ cm$^{-1}$ (1826−1924 cm$^{-1}$), $\Delta\nu_{Fe-CO} = 14$ cm$^{-1}$ (437−451 cm$^{-1}$), and $\Delta\nu_{C-O} = 9$ cm$^{-1}$ (1977−1986 cm$^{-1}$). The FeNO angle bends approximately 20° across the {FeNO}⁶ systems, while the FeCO moiety remains essentially linear.

Consistent with the HOMOs of the ImH complexes, the set of orbitals in Figure 9 also shows pronounced differences between the FeXO electron densities of the {FeNO}⁶ and [Fe^IICO] complexes. Figure 9A shows that the HOMOs-1 for the series of [Fe(P)(Im)NO] and [Fe(P)(Im)CO]$^-$ complexes are principally porphyrin $\pi$ MOs with electron density concentrated on the meso carbon and pyrrole nitrogen atoms. Also consistent with the behavior of the ImH complexes (Figure 8), the introduction of meso $\pi$-donor substituents

induces large redistributions of electron density toward the FeNO moiety. Such remarkable polarization of the HOMOs-1 is not observed in the corresponding [$Fe^{II}$CO] porphyrinates. This contrast is illustrated in Figure 9B,C for the P-*meso*-($NH_2$) and P-*meso*-($NH_2$, F)$_2$ systems, respectively. The HOMOs-1 of the [Fe(Por)(Im)NO] complexes take on increasing FeNO $\pi$-antibonding character as electron density is polarized toward the FeNO core. This increase in totally Fe−N−O $\pi$-antibonding character has the effect of simultaneously diminishing the Fe−NO and N−O bond strengths. Additionally, for [Fe(P-*meso*-($NH_2$, F)$_2$)(Im)NO] this orbital increases in energy to the extent that it becomes the HOMO. On the other hand, the very slight FeCO $\sigma$* character of the HOMO−1 is effectively constant among the [$Fe^{II}$(Por)(Im)CO]$^-$ series.

**1c. Basis Set Effects on Axial Ligand Bonding in [Fe(Por)(ImH)NO]$^+$ and [Fe(Por)(Im)NO].** Although we have pointed out that the larger 6-311G(2d,p) basis set yields only small effects on FeNO bond lengths and vibrational frequencies, it remains to determine whether the larger basis set influences the correlations among Fe−N−O bonding parameters and/or the molecular orbital analysis described above. Toward this end, geometry optimizations were performed on [Fe(P-*meso*-($NH_2$, $F_3$))(ImH)NO]$^+$ (Figure 8C) and [Fe(P-*meso*-($NH_2$, F)$_2$)(Im)NO] (Figure 9C) using the 6-311G(2d,p) basis set; the resulting FeNO parameters for these complexes are listed in Table 1. The results of these calculations, along with those for the unsubstituted porphine analogues, reveal that the direct correlations between Fe−NO and N−O bond lengths are also calculated with this basis set. In addition to the slopes ($\Delta R_{Fe-NO}/\Delta R_{N-O}$) from these sets of calculations being indistinguishable, the molecular orbitals (not shown) indicate the same electronic basis for the direct correlation between the strengths of the Fe−NO and the N−O bonds.

**2. Orbitals Responsible for the Indirect Correlation between Sensitivities of Fe−XO and X−O Bond Strengths to Structure and Environment.** The above orbitals qualitatively account for the *direct* correlations shown for {FeNO}$^6$ porphyrinates in Figures 3, 4, 6, and 7. However, they neither account for nor provide insight into the inverse correlations between Fe−XO and X−O bond strength correlations.

**2a. [Fe(Por)(ImH)NO]$^+$ and [Fe(Por)(ImH)CO].** Our recent work on five-coordinate {FeNO}$^6$ porphyrinates showed that they can exhibit either a large direct correlation between Fe−NO and N−O bond strengths or a small inverse correlation covering stretching frequency and bond length ranges similar to the corresponding [$Fe^{II}$CO] complexes.[9] The inverse correlation in {FeNO}$^6$ porphyrinates was observed for variations in the $\beta$-pyrrole substitution pattern at the porphyrin periphery. In these complexes, the only MOs in which FeNO electron density was significantly influenced by variations in $\beta$-pyrrole substituent pattern were those having Fe−NO $\pi$/N−O $\pi$* character, namely, the HOMO−(2,3) pair.

Careful examination of Figures 3 and 4 and Table 1 reveals that $\beta$-pyrrole-substituted systems (i.e., [Fe(P-$\beta$-$F_8$)(ImH)NO]$^+$ and [Fe(P-$\beta$-($NH_2$)$_4$)(ImH)NO]$^+$) behave in a manner distinct from their meso-substituted counterparts. The $\beta$-pyrrole-substituted systems cluster in the vicinity of the porphine complex in both the frequency and bond length correlation plots. Moreover, they appear to constitute a separate inverse correlation. In fact, the [Fe(Por)(ImH)NO]$^+$ $\beta$-inverse correlation for these two points has a $\Delta\nu_{Fe-NO}$ range of 17 cm$^{-1}$ (619−636 cm$^{-1}$) and a $\Delta\nu_{N-O}$ range of 16 cm$^{-1}$ (1971−1987 cm$^{-1}$), while the analogous two point $\beta$-inverse correlation for [$Fe^{II}$(Por)(ImH)CO] spans 15 cm$^{-1}$ (435−450 cm$^{-1}$) and 23 cm$^{-1}$ (2008−2031 cm$^{-1}$) for $\Delta\nu_{Fe-CO}$ and $\Delta\nu_{C-O}$, respectively. These sets of complexes cover very similar correlation ranges, suggesting similarity in the orbital basis of their correlations.

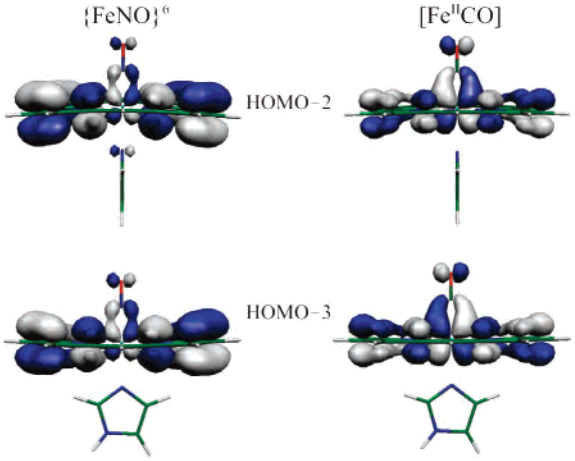


**Figure 10.** HOMO−2 and HOMO−3 for [Fe(P)(ImH)NO]$^+$ and [Fe(P)(ImH)CO] showing the Fe−XO $\pi$ and X−O $\pi$* character of these MOs.

In contrast to the large direct correlation in {FeNO}$^6$ complexes, the indirect correlation does not appear to be attributable to sensitivity of FeNO electron density within a single MO. There are a number of high-energy occupied MOs (i.e., HOMO−2, HOMO−3, HOMO−8, and HOMO−9 for [$Fe^{II}$(Por)(ImH)CO]) having Fe−CO $\pi$/C−O $\pi$* (back-bonding) character in these complexes, as illustrated for the HOMO−(2,3) pair of [FeP(ImH)NO]$^+$ and [FeP(ImH)CO] in Figure 10. However, changes in FeXO electron density are not apparent from examining the Kohn−Sham orbitals (not shown). This is not particularly surprising, given that the Fe−X−O bond strength sensitivities responsible for the small indirect correlations are distributed over multiple orbitals.

The large ranges of the direct correlation between Fe−NO and N−O bond strengths relative to those of the inverse correlation suggest that any changes in {FeNO}$^6$ porphyrinate structure and/or environment that influence FeNO electron density in the HOMO will cause the correlation to be direct. This analysis provides a consistent picture of the direct stretching frequency and bond length correlations for the ImH adducts of meso-substituted {FeNO}$^6$ porphyrinates.

**2b. [Fe(Por)(Im)NO] and [Fe(Por)(Im)CO]$^-$.** The HOMO−(5,6) pair of the [Fe(Por)(Im)NO] and [Fe(Por)(Im)CO]$^-$ complexes is the closest in FeXO character to the HOMO−(2,3) pair of their ImH counterparts. Again, however, these complexes comprise multiple high-energy MOs (i.e., HOMO−

2, HOMO−4, HOMO−5, and HOMO−6 for [Fe(Por)(Im)-CO]$^-$) having Fe−CO $\pi$/C−O $\pi^*$ character. Despite this commonality with their ImH counterparts, the imidazolate complexes of {FeNO}$^6$ porphyrinates do not appear to exhibit a separate inverse correlation for the $\beta$-substituted systems. Although the reason for this is not clear, it may be rooted in multiple orbital contributions to the relative sensitivities of the Fe−NO and N−O bond strengths. As suggested by the approximately vertical correlation for [Fe(P-$\beta$-$(NH_2)_4$(Im)-NO], [Fe(P)(Im)NO], and [Fe(P-$\beta$-$F_8$)(Im)NO], it is possible to have offsetting contributions such that the net contribution of a change in porphyrin $\beta$-pyrrole substitution to the change in N−O bond order is nearly zero while the Fe−NO bond strength remains responsive.

**3. Other Structural Sensitivities to Peripheral Substituents. 3a. Equilibrium Out-of-Plane Deformation of the Porphyrin Ligand.** Casual examination of Figures 8 and 9 reveals that the porphyrin ring adopts an increasingly ruffled conformation as the number and size of its meso substituents increase. Given the widespread interest in out-of-plane porphyrin deformations and their physicochemical manifestations, this trend warrants comment. Our previous calculations on five-coordinate porphyrins with the only axial ligands being NO or CO showed that ruffling is unlikely to be attributable to steric interactions between the porphyrin and these axial diatomic ligands. This was confirmed in this study by analysis of the resultant structures for constrained geometry optimizations of [Fe(P)(ImH)NO]$^+$ (Figure 5) where in the highly bent structure ($\angle$FeNO = 155.0°) becomes no more ruffled than the fully optimized structure (structures not shown). With the addition of an imidazole or imidazolate ligand to [Fe(P)NO]$^+$, the extent of ruffling increases slightly, the extent of which can be seen in Figures 2, 8A, and 9A. Thus the sixth imidazole ligand plays a minor role in ruffling. It appears that the most significant driving force for ruffling is the relief of steric interactions involving the peripheral porphyrin substituents. This is corroborated by comparing the extent of ruffling in P, P-*meso*-$F_4$, P-*meso*-$(NH_2)_2$, P-*meso*-$(NH_2)_3$, P-$\beta$-$(NH_2)_4$, and P-$\beta$-$F_8$, in both the imidazole and imidazolate complexes, which reveals that ruffling in these structures is driven by interactions between meso substituents and $\beta$-pyrrole hydrogen atoms. The extent of ruffling depends on meso substituents for the ferrous CO complexes in a similar fashion as it does for the ferric NO complexes. These observations are consistent with a large body of crystallographic and spectroscopic data showing that (a) axial imidazole planes oriented between pyrrole nitrogen atoms induce ruffling of the porphyrin ligand as a consequence of steric interactions and/or electronic stabilization and (b) steric interactions of peripheral porphyrin substituents can induce very large distortions along the ruffling coordinate.[55]

**3b. Core Deformations of Fe−N−O and Fe−$N_p$ Bonds.** Examination of Table 1 as well as Figures 2, 8, and 9 also reveals that increased $\pi$ donation from meso substituents elicits bending in the FeNO moiety and tilting of the Fe−NO bond away from the normal to the mean heme plane and in the same direction as the bend. As will be discussed below, these distortions occur in response to buildup of FeNO electron density in the HOMO or HOMO−1. Similar distortions occur in response to buildup of FeNO electron density in the HOMO or HOMO−1 due to increasing $\sigma$ donation by a trans axial ligand, as can be seen by the decreased $\angle$FeNO in [Fe(P)(Im)NO] (Figure 9A) relative to the nearly linear FeNO unit in [Fe(P)(ImH)NO]$^+$ (Figure 8A). The FeNO distortions are accompanied by the appearance of asymmetry in the Fe−$N_p$ core. The Fe−$N_p$ distances listed in Tables 1 and 2 show that this asymmetry tracks inversely with $\angle$FeNO. In all cases, decreasing $\angle$FeNO, either by imposing $\angle$FeNO < 180° (Table 2) or by polarizing electron density toward FeNO in the HOMO of the ImH complexes (vide infra, Table 1), causes inverse changes in the lengths of opposing Fe−$N_p$ bonds, with the iron atom shifting in the opposite direction of the FeNO tilt and bend. When decreasing $\angle$FeNO is imposed on the complex, the distance between opposing $N_p$ atoms decreases by 0.004 Å as $\angle$FeNO is decreased from 179.7° to 155.0° (Table 2). This is attributed to a slight increase in the out-of-plane distortion along the ruffling coordinate as the FeNO moiety is bent. The bond lengths in Table 2 indicate that this is not a direct effect of steric interaction between the bent NO ligand and the porphyrin; in fact, the distance between the terminal oxygen atom and the porphyrin *decreases* as the Fe−NO bond gets longer with increased ruffling. The increased ruffling that accompanies the decrease in porphyrin core size is an indirect effect of systematic Fe−ImH bond shortening as the Fe−NO bond becomes weaker due to FeNO bending. The shorter Fe−ImH bond increases the steric interactions between the axial ImH and porphyrin ligand, thereby increasing the ruffling distortion. This inverse correlation between the Fe−ImH and Fe−NO bond distances is clearly shown by the plots in Figure 11. They show virtually the same correlation lines, whether the off-axis distortions are imposed by constraining them or electronically driven by polarizing electron density toward FeNO in the HOMO. A similar inverse correlation is not seen for

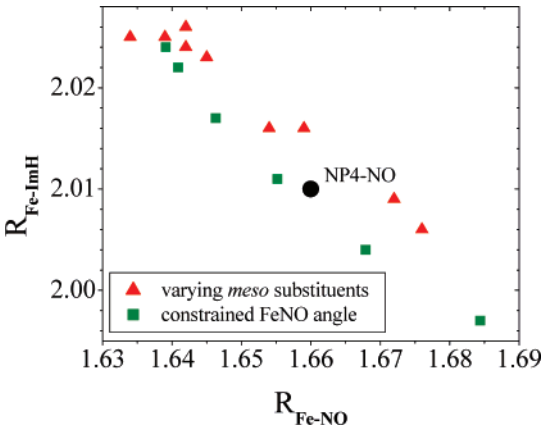


**Figure 11.** Correlation between B3LYP/6-31G(d)-optimized Fe−ImH and Fe−NO bond lengths for varying meso substituents in [Fe(Por)(ImH)NO]$^+$ complexes (▲, constructed from data in Table 1) and for constrained $\angle$FeNO calculations (■, constructed from data in Table 2). The point corresponding to NP4−NO (●) was placed according to crystal structure coordinates.[24]

(55) Ellison, M. K.; Schulz, C. E.; Scheidt, W. R. *J. Am. Chem. Soc.* **2002**, *124*, 13833−13841.

analogous $Im^-$ complexes, possibly because the HOMO and HOMO−1 exchange character with respect to axial ligand interactions when the FeNO moiety becomes electron rich.

The effects described above have been observed experimentally to varying degrees. Two structurally characterized systems will be considered here. Examination of the high-resolution NP4−NO crystal structure shows ruffling of the $\{FeNO\}^6$ heme similar to that seen in all of the DFT-optimized structures reported here. Although out-of-plane distortion of the heme in NP4−NO also occurs along the saddling coordinate, it is dominated by ruffling that appears to be synergistic with the side chain positions of the distal Leu residues that make van der Waals contact with the axial NO ligand. The extent of ruffling and saddling distortions both increase upon replacement of an axial water or ammonia ligand by NO.[24] As suggested by the constrained geometry calculations reported here, these increases in out-of-plane heme distortion are likely attributable, at least in part, to increased steric interactions due to closer approach of a strongly bound proximal ImH ligand to the mean porphyrin plane in NP4−NO. However this is not unambiguous, as the difference in ImH approach is on the order of the experimental uncertainty in the bond distances. Core asymmetry cannot be discerned due to uncertainty in the $Fe-N_p$ distances.

Another six-coordinate $\{FeNO\}^6$ porphyrinate having a conspicuously bent FeNO moiety is [Fe(OEP)(*p*-$C_6H_4F$)NO], in which ∠FeNO = 157.4°.[53] Although this complex contains a different ligand trans to NO, it is a high-resolution structure that lends itself to detailed analysis of FeNO bonding parameters. This complex exhibits Fe−NO tilting and bending, Fe−(*p*-$C_6H_4F$) tilting, and core asymmetry analogous to that observed in the $[Fe(Por)(ImH)NO]^+$ complexes presented herein. Although this complex does not contain peripheral $\pi$ donor substituents to polarize electron density toward the FeNO moiety, it does contain the strongly $\sigma$ donating *p*-$C_6H_4F$ aryl ligand. The fact that the ∠FeNO is so small strongly suggests that the aryl ligand induces substantial FeNO $\pi^*$ character in a MO in the frontier region. In this situation, FeNO bending and tilting are expected in order to partially compensate for the increased FeNO antibonding. This complex also exhibits significant asymmetry of the porphine core with the $Fe-N_p$ bonds nearest to the bent NO ligand being longest. This is consistent with the asymmetry calculated for the various substituted porphyrinates (Table 1) and for the enforced changes in ∠FeNO (Table 2).

Having established by these comparisons that the calculated bonding parameters listed in Table 1 are meaningful, we now proceed to a discussion of two Kohn−Sham orbitals to which these first coordination sphere distortions can be attributed. There appear to be two MOs relevant to FeNO distortion and equatorial asymmetry. They are most easily identified in the constrained geometry optimization of $[Fe(P)(ImH)NO]^+$ with ∠FeNO constrained to 155.0°, as illustrated in Figure 12. The images in Figure 12A,B show edge-on and top views, respectively, of the HOMO−1. In the 155° constrained geometry calculation for [Fe(P)(ImH)-

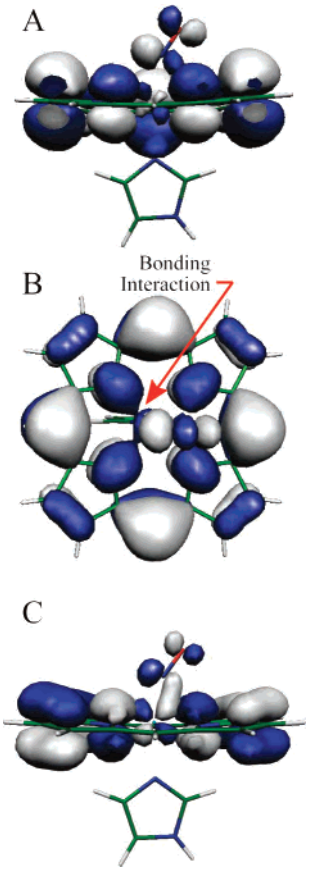


**Figure 12.** MOs showing the interplay between ImH−Fe−NO character of the HOMO−1 and HOMO−3 and ImH−Fe−NO distortions, equatorial $Fe-N_p$ asymmetry, FeNO bending and off-normal Fe−NO tilt for $[Fe(P)(ImH)NO]^+$ having ∠FeNO constrained at 155°. (A) HOMO−1, edge-on view with electron density at the front edges removed to facilitate viewing of the FeNO moiety; (B) HOMO−1, top view; and (C) HOMO−3, edge-on view.

$NO]^+$, HOMO and HOMO−1 are reversed from their order in all other ImH complexes studied here. The reason for the reversal is not clear at this point. The center of Figure 12A reveals an Fe-centered $d_{z^2}$-like contribution to HOMO−1 that is slanted in the opposite direction of the FeNO tilt and bend. This electron density along with that on the NO ligand contributes to a totally $\pi$ antibonding character of the HOMO−1 with respect to FeNO. At the same time, it contributes to Fe−ImH bonding character. Thus any electronic or structural perturbation of the axial ImH−Fe−NO "stem" of the molecule will simultaneously weaken the Fe−NO bond and strengthen the Fe−ImH bond. A reason for Fe−NO bending and tilting will be discussed below, but there are two structural properties that are intimately intertwined with bending and tilting. The first is a slight off-normal tilt of the Fe−ImH bond in the direction of the FeNO tilt. This maximizes the Fe−ImH bonding character of the HOMO−1. The second is a core asymmetry, which tracks ∠FeNO. Tilting of the $d_{z^2}$-like contribution to HOMO−1 leads to two $Fe-N_p$ antibonding interactions in the direction of the FeNO bend and two bonding interactions on the other side of the NO ligand. Figure 12B shows the bonding interactions. These interactions result in simultaneous lengthening of two adjacent $Fe-N_p$ bonds and shortening of their trans coun-

terparts, resulting in an ∠FeNO-dependent shift of the Fe atom in the mean porphyrin plane and away from the NO ligand. While there may be other MOs or groups of MOs that contribute to these structural relationships, they are clearly rationalized in terms of the electron density distribution in the HOMO−1 and the systematic redistribution thereof in response to changing structure and/or environment.

The question of why the ImH−Fe−NO stem of the molecule becomes increasingly distorted with increasing electron density still remains. Table 1 reveals that the Fe−NO bond is weakened, as gauged by its increased length, with the introduction of $\pi$ donor substituents at the meso carbons of the porphyrinate ligand, which is attributed to the totally antibonding FeNO character of the HOMO. Interestingly, the same effect is observed upon enforced bending of the FeNO moiety, as shown in Table 2 and Figure 11. This loss in Fe−NO bond order is partially compensated by an axially asymmetric Fe−NO bonding interaction in the HOMO−3 that is facilitated by bending and tilting of the FeNO moiety as well as slanting of a $d_{xz}$-type contribution to HOMO−3. Such bonding character would likely be quite weak or nonexistent in a linear FeNO unit having a long Fe−NO bond. This Fe−NO bonding character is illustrated in Figure 12C, which shows an edge-on view of HOMO−3 for $[Fe(P)(ImH)NO]^+$ with ∠FeNO constrained at 155.0°. It is interesting to note that the FeNO electron density in fully minimized $[Fe(P)(ImH)NO]^+$ (Figures 8A) and in that with ∠FeNO fixed at 155.0° (Figure 12A) differ substantially. Enforcing a bend in the FeNO moiety increases the off-normal Fe−NO tilt, the FeNO electron density, and Fe−N−O distances. On the other hand, by changing the $\pi$ donor ability of porphyrin meso substituents in such a way as to concentrate electron density on the FeNO moiety, ∠FeNO decreases, off-normal tilt increases, and Fe−N−O distances increase. Additionally, the inverse correlation between Fe−NO and Fe−ImH bond lengths is observed for both types of perturbation (Tables 1 and 2). Taken together, these results clearly show that the cause-and-effect relationship between FeNO geometry and NO electron density in the higher occupied MOs of {FeNO}$^6$ porphyrinates (and the consequent changes in Fe−NO and N−O bond strengths) is bidirectional. Hence, whether FeNO electron density is increased by changes in peripheral substituents (cis effects), by changes in proximal donor strength (trans effects), or by enforced bending (steric effects), the concerted responses of the FeNO geometry and bond strengths remain consistent. These calculations reveal an exquisite sensitivity of NO electron density within MOs in the frontier energy region to enforced structural changes or polarization effects such as those imposed by bonded and nonbonded heme−protein interactions in the heme pockets of proteins and enzymes. Thus it is reasonable to suggest that such sensitivity provides considerable control over the reactivity of NO toward oxidation, reduction, and dissociation in {FeNO}$^6$ porphyrinates.

Recent discussions of the NP4−NO crystal structures have cast some doubt upon the assignment of the heme as a {FeNO}$^6$ species. Because of the rather small FeNO angle, the possibility of the heme having been reduced to {FeNO}$^7$ in the X-ray beam has been set forth.[7] The intrinsic stability of bent {FeNO}$^6$ porphyrinates and the small cost of bending the FeNO moiety revealed by the results presented here clearly support the possibility of a highly bent {FeNO}$^6$ porphyrinate having a neutral proximal imidazole ligand. Moreover, the direct relationship between NO electron density within the HOMO and ∠FeNO supports the hypothesis that enforcement of this small angle by the protein is the means by which reductive nitrosylation, which would render the protein useless as an NO delivery vehicle, is precluded. If this hypothesis is borne out, the proposed attack of hydride on the nitrogen atom of {FeNO}$^6$ hemes in NO reductase reactions would be favored by an electron-deficient NO ligand. The results presented here suggest that, based on electronic considerations alone, if P450nor-catalyzed NO reduction involves hydride attack on the nitrogen atom of {FeNO}$^6$, it would best be facilitated by a more electron-deficient, linear {FeNO}$^6$ moiety. Interestingly, the structures of fungal P450nor−NO indicate a bent FeNO moiety with ∠FeNO ≈ 160°.[13] There is but one steric interaction between the backbone carbonyl of Ala 239 and the NO ligand, which might play a role in enforcing an FeNO bend. The bent structure is also likely to be stabilized by strong donation by the proximal Cys-based thiolate ligand, analogous to that observed for the aryl ligand of [Fe(OEP)(*p*-$C_6H_4F$)NO] and for the $Im^-$ complexes studied here. A bent and, therefore, electron-rich NO ligand would make it less susceptible to attack by nucleophiles such as water and hydroxide. While this could serve to protect the heme against reductive nitrosylation, it would also be expected to diminish the kinetic efficacy of hydride transfer to bound NO. Hence, as one might expect, it appears that explanation of structural and mechanistic data for NO reduction will require a unified understanding of the interplay between static and dynamic aspects of the protein environment and intrinsic electronic properties of the heme−NO complex. For example, the NO could be released from its bent geometry in response to a conformational transition triggered by NADH binding. This could occur by relaxation of the interaction between bound NO and Ala239 and/or by protonation of the proximal Cys-based thiolate ligand which, by analogy to protonation of the $Im^-$ ligand in [Fe(P)(Im)NO], would render the bound NO less bent and more electron deficient. Such an NADH-triggered change in FeNO structure and bonding would explain how the bound NO can be reduced by hydride transfer while being protected from reductive nitrosylation in the rather solvent exposed heme pocket of P450nor−NO.

## Conclusions

In this study we present DFT calculations on a series of model six-coordinate {FeNO}$^6$ porphyrinates that contain either an axial ImH or $Im^-$ ligand trans to NO. The results of geometry optimizations and force constant calculations show that indicators of Fe−NO and N−O bond strengths (vibrational stretching frequencies and bond lengths) are *directly* correlated in both classes of complexes. An analysis of Kohn−Sham orbitals shows that this direct correlation

results from structural and environmental sensitivities of the FeNO electron density within the HOMO or HOMO−1, which are $\pi$ antibonding with respect to the entire FeNO triatomic unit. In addition to the large direct correlation for both systems, we also propose that the responses of Fe−NO and N−O bond strengths are inversely correlated over smaller ranges, similar to those of the FeCO correlations, for groups of $[Fe(P)(ImH)NO]^+$ complexes with varying $\beta$-pyrrole substitution patterns. This relationship is not seen among the [Fe(P)(Im)NO] analogues. Orbital analysis further reveals that the axial ligand distortions in these complexes also occur in response to the sensitivities of electron density distributions within the HOMO or HOMO−1, and HOMO−3. The overarching theme emerging from this work is that the Fe−N−O bond strengths in $\{FeNO\}^6$ porphyrinates are susceptible to modulation over a considerable range and that FeNO $\pi$-antibonding electron density and FeNO geometry, as modulated by distal, cis, and trans effects, are tightly coupled such that perturbation of one causes the complementary change in the other. This interplay between distortions in the axial stem of $\{FeNO\}^6$ porphyrinates and their electronic properties provides insight into how, and the extent to which, protein environment can influence the reactivities of heme-bound NO toward nucleophiles such as water, hydroxide, and hydride.

**Acknowledgment.** The authors acknowledge access to the Computational Chemistry and Biology Network (CCBN) and the Center for High Performance Computing (CHPC) at NDSU, where the calculations were performed (NIH RR-16471). Financial support from USDA (ND05299, K.R.R.), the Hermann Frasch Foundation (446-HF97, K.R.R.), and NCRR (P20 RR15566, K.R.R.) is also gratefully acknowledged. Finally, the authors thank Professor W. Robert Scheidt for insightful discussions.

**Supporting Information Available:** Table S1 containing calculated bonding parameters for the CO complexes. This material is available free of charge via the Internet at http://pubs.acs.org.

IC049045H